PHYSICAL REVIEW B VOLUME 30, NUMBER 4 15 AUGUST 1984

Laser-induced periodic surface structure. III. Fluence regimes, the role of feedback, and details of the induced topography in germanium

Jeff F. Young, J. E. Sipe, and H. M. van Driel
Department of Physics and Erindale College, University of Toronto, Toronto, Ontario, Canada M5S 1A7
(Received 26 January 1984)

The mechanisms responsible for the growth of periodic surface structure on Ge irradiated by 1.06-μm laser pulses from a single beam are investigated. Time-resolved diffraction of a weak cw probe beam from the developing structures, coupled with electron-microscope pictures of the resulting morphology, is used to identify four distinct regimes of ripple formation at different incident laser fluences. At low fluences, the structure develops when thin (<1 μm wide) isolated, molten strips resolidify on the solid substrate, while at high fluences, the structure results from freezing of capillary waves which are generated on the surface that the laser pulse has melted uniformly. Models are presented which clearly demonstrate how the incident electromagnetic field interacts with the evolving structures (in different fluence regimes) to provide feedback mechanisms which sustain their growth.

I. INTRODUCTION

An investigation into the mechanisms whereby pulsed-laser energy is deposited near the surface of a material is important for understanding such phenomena as laser damage and laser material processing.[1] In most of the research reported over the past two decades, the laser is often considered simply as an ultrafast heat gun which is capable of locally heating the subsurface region of the material. One-dimensional (depth) models have successfully[2-9] been used to explain many aspects of the interaction. In general, the role of (a) laser coherence and polarization and (b) the surface morphology in influencing energy deposition is not considered. However, it has been known since the early days of the laser that the energy-deposition process can be spatially inhomogeneous[5,6] and, under certain conditions, periodic energy deposition can induce periodic surface structure[7-14] on a wide variety of materials. Owing to the importance of these effects and the general interest[15-17] in two-dimensional surface processing of materials (such as in direct writing of structures), we have undertaken fundamental investigations of the effect of beam coherence and polarization on surface processing. During the course of these investigations, several other groups have also considered models for this interaction.[18-21] In the first of the previous two papers[22,23] of this series (referred to as I and II hereafter), we presented a theoretical understanding of how the laser properties and surface roughness can lead to spatially periodic energy deposition, and offered predictions of the spatial spectra of the structures for different angles of incidence and beam polarization. Most of these features were verified experimentally in paper II for several semiconductors and metals which had been illuminated with 1.06- and 0.53-μm, 20-ns pulses. The common characteristics observed on semiconductors, metals, and insulators,[13,24] and solids and liquids,[25] led us to conclude that laser-induced periodic surface structure (LIPSS) by single laser beams is a universal phenomenon[26] that can occur on any material that absorbs radiation, regardless of its dielectric constant.

The aim of this paper is to address the dynamical processes associated with LIPSS by considering the coupled material—electromagnetic-field interactions. We consider the detailed evolution of the surface topography; in particular, we investigate how inhomogeneous melting and material flow influence and are influenced by the surface electromagnetic fields. The role of feedback in the growth of the structures is considered both in the intrapulse and interpulse sense for multiple shots. We show that for fluences near the threshold for LIPSS formation the surface structure evolves from a periodic array of molten strips. At higher fluences, periodic structures are also formed even though the material/air interface melts uniformly. This occurs through the excitation of capillary waves at the liquid/air interface, which then freeze as the material resolidifies. In all, four qualitatively different regions of LIPSS formation are identified through the use of time-resolved optical-diffraction, electron-microscope, and optical-microscope studies of the surface topographies. Laser diffraction from the surfaces has also been used to identify how the fluence of the 1.06-μm pulses influences the spacings of the induced structures, which reflect the changes in the optical properties of the surface.

In the work reported here, only the interaction of Ge with 20-ns, 1.06-μm pulses is considered as a prototypical situation, since many of the effects considered are universal in character. However, the *detailed* growth characteristics and material flow may be different in different materials. It might also be noted that the spatial spectra (the main subject of papers I and II) are largely independent of feedback considerations and the dynamics of growth. The situation is somewhat analogous to Raman spectroscopy, where similar spectra are obtained under spontaneous and stimulated scattering conditions.

The remainder of the paper is organized as follows. In Sec. II we consider the experimental apparatus and tech-

niques used in the investigations. In the following section we consider the four distinct fluence regions of LIPSS formation and show the time-resolved characteristics, spacings, and morphology of each regime. In Sec. IV we experimentally and theoretically consider the role of inter- and intrapulse feedback for certain illumination conditions. Finally, the results are summarized and put in perspective with respect to the work of other investigators in Sec. V.

II. EXPERIMENTAL TECHNIQUES

In the investigations reported here, germanium samples had periodic structures induced on them by single or multiple 20-ns [full width at half maximum (FWHM)] pulses by a 1.06-μm, Q-switched Nd:YAG (where YAG denotes yttrium aluminum garnet) laser. The real-time evolution of the structures was monitored by simultaneously observing the zeroth- (specular reflectivity) and first-order diffraction characteristics of a 0.51-μm cw Ar^+-ion laser beam which illuminated the irradiated region. The correlation of these two signals gave detailed information about the thermal phase of the surface, its spatial homogeneity, and, in general, detailed information about the temporal evolution of the surface morphology. Post-irradiation diagnostics were performed using either a phase-contrast (Nomarski) optical microscope or a scanning electron microscope (SEM). In this section we will briefly outline the sample characteristics and experimental techniques used to obtain the data reported later.

Both single-crystal and polycrystalline intrinsic germanium samples were used in the studies. They were either polished with diamond pastes with grit sizes down to 0.25 μm or polished then etched with a standard CP4-A etch solution. There were no significant differences noted in the transient evolution of the periodic structures or their final form for the different samples. It should be noted, however, that the sample surfaces were prepared within 6 h prior to any transient-response experiment in order to guarantee reproducible results. Samples left overnight displayed highly irreproducible reflectivity and diffraction signals, particularly during the first few shots. This phenomenon is most likely due to the formation of thick (>30 Å) oxide layers on the germanium surfaces, since it has been recognized for several years that germanium surfaces are not easily passivated.[27]

Figure 1 schematically illustrates the most general optical configuration used to obtain information about the optical properties of the surface, during LIPSS formation on a nanosecond time scale. Although not all of this apparatus was used in each of the experiments, the general case facilitates a thorough discussion of all the components which are referred to in subsequent sections. The characteristics of the Nd:YAG laser were described in paper II. To obtain smoothly varying spatial-intensity profiles, a small, less than 2-mm-diam aperture, $A1$, was placed at the output of the laser so as to obtain a uniform region of the most intense portion of the spot (cross section of 1 cm^2). Only the central portion of the far-field Airy pattern was directed through a Glan-Taylor polarizer, GL1, and allowed to impinge upon the sample surface.

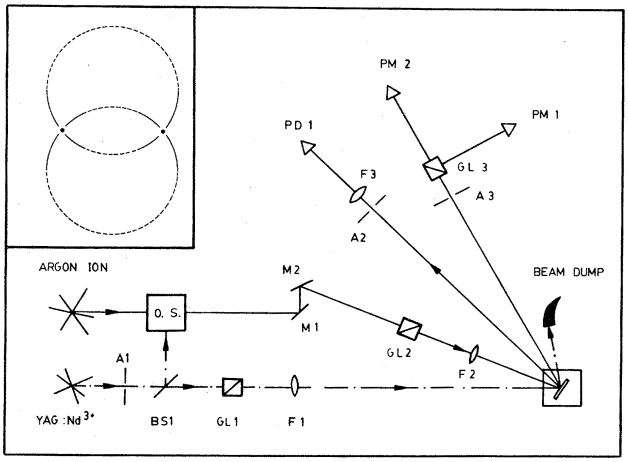

FIG. 1. Schematic diagram of the most general optical setup used to perform the transient diffraction experiments. The box marked OS represents the optical switch; the elements are described in detail in the text. The inset is a schematic diagram of a typical diffraction pattern.

To maintain this spatial uniformity, no additional optics were used, except to obtain incident fluences higher than 300 mJ/cm^2. In such cases the beam was focused onto the sample by inserting a simple lens of focal length 15 cm after the polarizing element. The sample was mounted in ambient conditions on a micropositional stage which allowed for horizontal and vertical translation as well as rotation about horizontal and vertical axes.

The 0.51-μm Ar^+ probe laser was operated at powers below 300 mW/cm^2. In order to temporally correlate the zeroth- and first-order diffracted signals, a short timing "glitch" was superimposed on the cw beam before it diffracted from the sample surface. To achieve this, the beam was passed through an optical switch and delay line. The switch consisted of a Glan-Taylor prism in line with a Pockels cell which was activated by a high-voltage pulse from a spark gap triggered by a 1.06-μm pulse. The delay, required so that the synchronization pulse did not overlap the diffraction signals, was provided by a White cell.[28] Upon exiting the switch section, the beam was directed by mirrors, $M1$ and $M2$, so that it could impinge on the sample surface at any angle with respect to the fringes which were to be formed. From mirror $M2$, it passed through a Glan-Taylor prism, GL2, which defined the polarization of the beam with respect to the fringes, and a lens, $F2$, which focused it onto the sample surface. The spot diameter of the probe beam at the surface was 150 μm so that it covered a region of the sample over which the fluence of the pulsed beam was uniform. The diverging, specularly reflected beam passed through an aperture $A2$ and was focused by a lens $F3$ onto a silicon photodiode PD1 through a set of bandpass filters for the 0.51-μm beam. A portion of the first-order diffraction pattern from the damaged sample passed through an aperture, $A3$, and then through an analyzer, GL3, which passed the vertically polarized component and directed the horizontally polarized component towards an appropriately filtered photomultiplier, PM1. The vertically

polarized component was detected with a second photomultiplier, PM2. The signals from the photodetector and one of the photomultipliers were passed to a dual-channel storage oscilloscope, while the signal from the other photomultiplier was recorded on a second storage oscilloscope. In all cases, the time response of the photodetector-oscilloscope recording channels was experimentally determined to be better than 5 ns.

The samples were studied after the transient experiments using the optical and scanning electron microscopes. All the SEM work was done with single-crystal germanium samples. To determine the profile of the ridges which make up the induced microstructure, samples were prepared so that they could be viewed in plane view as well as in cross section. A thin wafer from the (111) surface of a single-crystal cylindrical slug was thinned to less than 90 μm at which point it was polished in the usual fashion. It was then mounted in such a way that when irradiated by the pulsed laser, the induced fringes were oriented perpendicular to the crystal plane. The damaged wafer was then cleaved parallel to a crystal axis and perpendicular to the fringes.

III. REGIMES OF LIPSS

In this section we characterize the development of LIPSS, relying heavily on experiments designed to correlate the specular reflectivity and first-order diffraction signals. These experiments were done using the general optical layout of Fig. 1, except that the two prisms GL2 and GL3 were omitted. The Ar^+ laser beam was near normally incident on the sample with its electric field vector oriented parallel to the Fourier vector of surface roughness which the photomultiplier was positioned to monitor.

In paper II we noted that the overall morphology of surface structure induced—that is, the spacing(s) and orientation(s) of fringes formed—depends critically on the angle of incidence and polarization of the damaging, or "pump" pulse. Interestingly, we found here that the results of the transient correlation experiments are remarkably independent of those parameters, indicating that the same basic mechanisms are involved in producing a host of different surface morphologies. However, the form and evolution of the correlated diffraction and reflectivity signals do change significantly as a function of the incident pump fluence. In fact, we could identify four qualitatively distinct fluence regimes of LIPSS, which we have labelled A—D in order of increasing fluence. The only effect of varying beam parameters such as polarization and angle of incidence is to change the value of fluence at which one crosses from one regime to the next; this is not surprising since the reflectivity of the pump beam, e.g., depends on these parameters. Our discussion in this section is aimed at establishing and describing the four different fluence regimes; we present results at angles of incidence and polarizations which were experimentally convenient to obtain.

Figures 2(a)—2(d) show typical sets of zeroth- and first-order diffracted signals characteristic of the four qualitatively different fluence ranges we observe. They were all obtained with an s-polarized 1.06-μm beam incident on the germanium at 30°; for these parameters the respective fluence ranges are, approximately, A, 120—200 mJ/cm^2; B, 200—220 mJ/cm^2; C, 220—450 mJ/cm^2; and D, 450—550 mJ/cm^2. The delayed spikes which appear on the oscilloscope traces in Figs. 2(a) and 2(b) are synchronization pulses used to temporally correlate the zeroth- and first-order signals. A schematic diagram of the complete diffraction pattern produced under these illumination conditions[29] is shown as an inset to Fig. 1. The aperture, $A3$, in front of the photomultiplier was positioned at the bright dot in the diffraction pattern to obtain the signals shown in Fig. 2. When this aperture was placed anywhere off the overlapping circular diffraction pattern, no transient signals were observed.

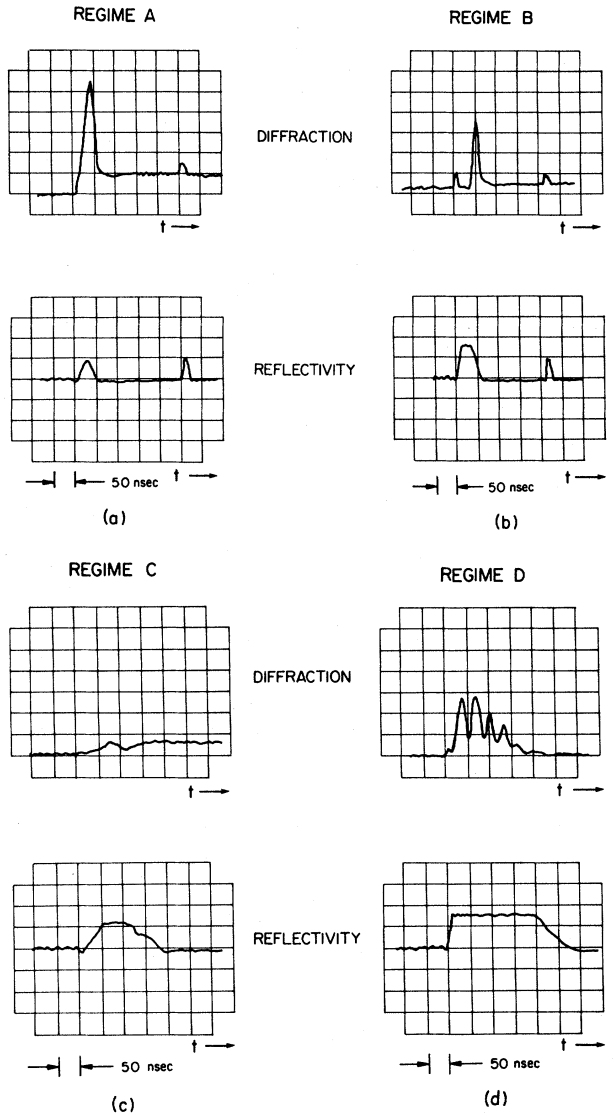

FIG. 2. Transient first-order diffraction and specular reflectivity of a 0.51-μm probe beam from a germanium surface irradiated at 30° by an s-polarized 1.06-μm pulse in the different fluence regimes indicated. The first-order diffraction was monitored at the bright dot in the diffraction pattern as shown in the inset of Fig. 1. In (a) and (b) the small spike approximately 200 ns after the main signal is the synchronization pulse imposed on the 0.51-μm beam with the optical switch indicated in Fig. 1.

A. Regime *A*

We first consider, in detail, regime *A*, which is characterized by the fact that the specular reflectivity never reaches the value of 75% characteristic of a uniformly molten surface. The dielectric constants of solid and liquid germanium at the wavelength of the probe beam, 0.51 μm, are $\epsilon_s = 22 + i23$ and $\epsilon_l = -20 + i23$, respectively,[30,31] leading to theoretical reflectivities of uniform solid and liquid half-spaces of 52% and 75%, respectively. If the laser caused the surface to quickly melt to a depth greater than the skin depth of the probe beam, i.e., to ~ 200 Å, one would expect the specular reflectivity to abruptly change from 52% to 75%, as it in fact does in regime *D* [see Fig. 2(d)]. The fact that the specular reflectivity in regime *A* does not rise to the 75% level might be interpreted in two ways. Perhaps only a very thin layer of material, less than the skin depth of the probe beam, melts uniformly, or perhaps only a small fraction of the surface area melts inhomogeneously. Ehrlich, Brueck, and Tsao,[18] who made similar transient measurements, based their explanation of the phenomena on the former interpretation. However, for a number of reasons, we believe that the less than 75% reflectivity is in fact due to inhomogeneous melting of the germanium surface.

First, consider the induced surface microstructure, as observed with an electron microscope. For fluences of the 1.06-μm beam corresponding to regime *A*, the permanent ridges formed on the material surface are always very localized, regardless of the incident angle or polarization. Figure 3 shows a cross-sectional view of the fringes formed by a *p*-polarized beam incident at 60° in regime *A*. The topographical view of fringes formed by *s*-polarized light incident at 30°, as shown in Fig. 4 as well as the other figures, is clearly consistent with the assumption that the material melts locally in periodic strips. In fact, we shall show in the next section that a periodic molten surface would indeed, upon resolidification, lead to precisely the "sombrero-shaped" periodic structure observed in Fig. 3. At a slightly higher fluence, but still within regime *A*, the width of the perturbed region is wider, but the localization is still apparent, as shown in Fig. 5.

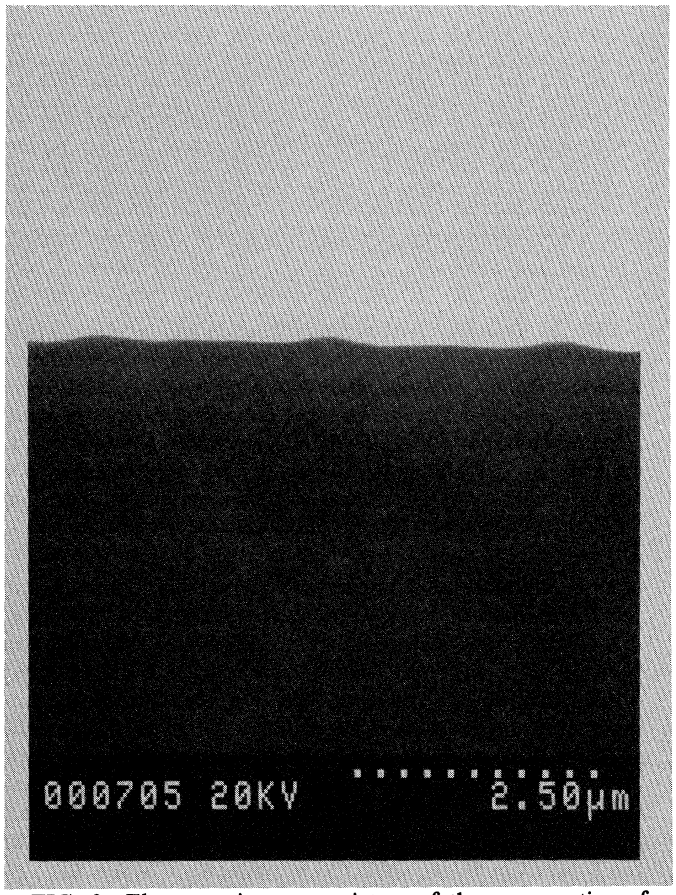

FIG. 3. Electron-microscope picture of the cross section of fringes formed by *p*-polarized, 1.06-μm pulses incident on germanium at 60° in regime *A*.

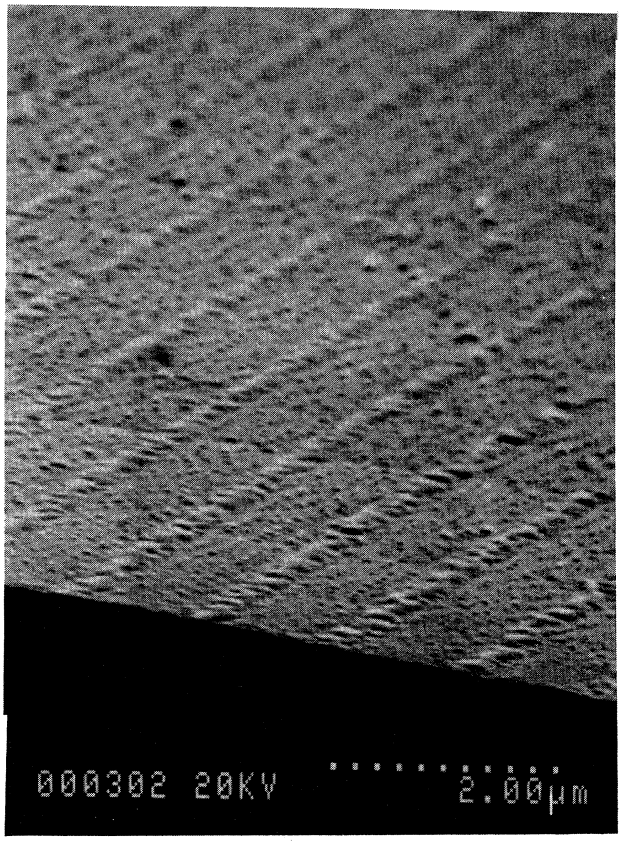

FIG. 4. Electron-microscopic picture of fringes formed by 20 *s*-polarized pulses of 1.06-μm radiation incident at 30° in fluence regime *A*.

Second, and perhaps most convincing, the results obtained from comparing the *s*- and *p*-polarized components of the probe beam's diffraction efficiency clearly indicate that the surface melts only locally in regime *A*. To compare these components, the prism GL2 (see Fig. 1) was oriented at 45° to the plane of incidence. The beam incident on the sample was thus a superposition of equal-amplitude *s*- and *p*-polarized components with relative phases such that it was linearly polarized. Since the plane of incidence was perpendicular to the fringes, the *s*- and *p*-polarized components of the first-order diffracted beam could be separated with a second prism, GL3, situated in, and oriented parallel to, the plane of incidence. The sig-

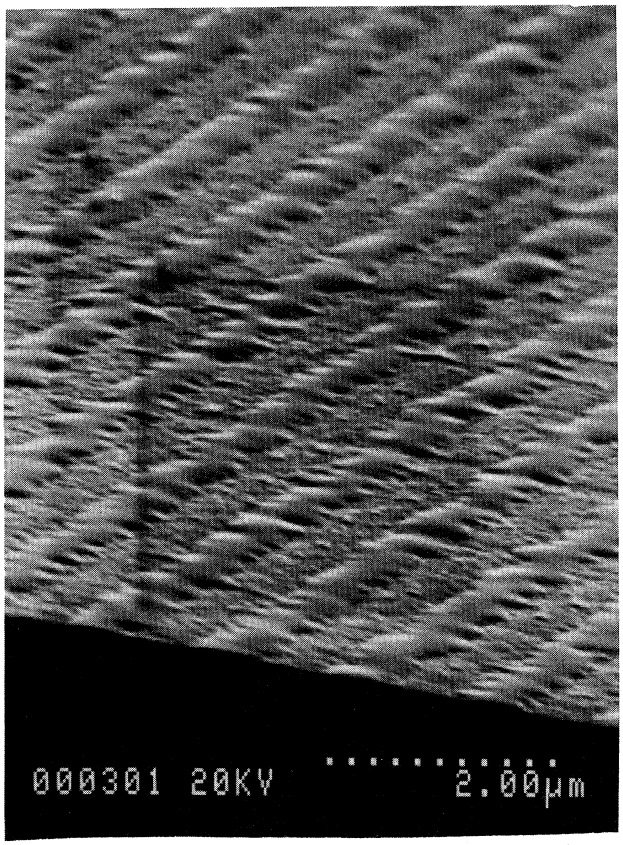

FIG. 5. Electron-microscopic picture of fringes formed under the conditions of Fig. 4, but at higher fluence, although still in regime *A*.

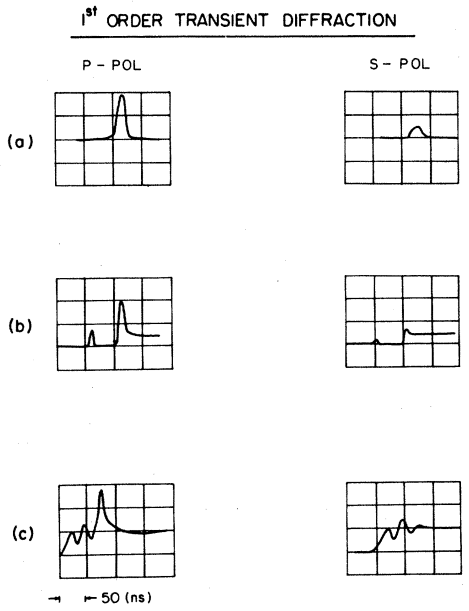

FIG. 6. First-order transient diffraction of the *p*-polarized (left) and *s*-polarized (right) components of a 0.51-μm probe beam incident on germanium at 60° with the plane of incidence perpendicular to the dominant set of fringes formed on the surface. The surface was simultaneously irradiated with an *s*-polarized 1.06-μm pulse incident at 30° and the first-order diffraction was monitored at the bright spot of the diffraction pattern shown in Fig. 3. The fluence of the 1.06-μm beam corresponded to regime *A* in (a), regime *B* in (b), and to a combination of regimes *D* and *B* in (c).

nals from the two polarized diffracted beams were detected by two photomultipliers and recorded on oscilloscopes, with the specular component still focused onto the photodiode so that it could be observed alternately with one of the diffracted signals.

With the Ar^+-laser beam near normal incidence, the *s*- and *p*-polarized transient diffracted signals were identical to within the 5% error associated with measurements from oscilloscope traces. With the Ar^+-laser beam incident at 60°, the results were quite different for the two polarizations. In regime *A*, the transient amplitude of the *p*-polarized diffracted beam was consistently 3.3 to 4.0 times larger than that of the *s*-polarized component, while the small permanent level shifts were identical [Fig. 6(a)]. To interpret the experimental results, a numerical diffraction-efficiency algorithm developed by Vincent, Neviere, and Maystre[32] was used to calculate the diffraction efficiency of the probe beam from a variety of periodically modulated surfaces as a function of incident angle. The results for a modulated liquid surface, and for a locally molten surface, are plotted in Figs. 7 and 8. We also performed calculations for a modulated solid surface, and a modulated liquid layer above a solid surface. At normal incidence, the ratio of *p*- to *s*-polarized diffraction efficiency for the modulated solid surface is within 10% of the same ratio for all of the other geometries. The gain of the photomultipliers was adjusted so that the *s*- and *p*-polarized components of the diffraction from the permanent structures (modulated solid surfaces) were equal; thus the fact that all the transient signals (in regimes

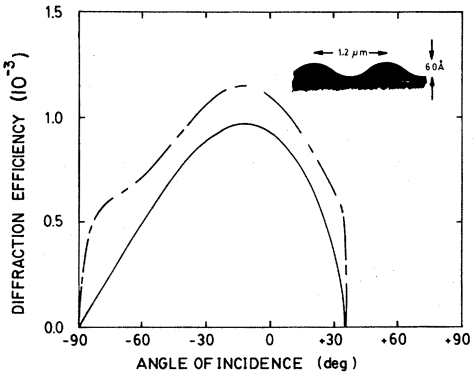

FIG. 7. First-order diffraction efficiency of a 0.51-μm probe beam from a modulated liquid-germanium surface, as depicted in the inset. The plots were calculated as a function of the angle of incidence of the probe beam, using the algorithm of Vincent *et al.* (Ref. 32). The dielectric constant of liquid germanium at 0.51 μm is $\epsilon_l = -20 + i23$. The solid line is for an *s*-polarized probe beam and the dashed line is for a *p*-polarized probe beam.

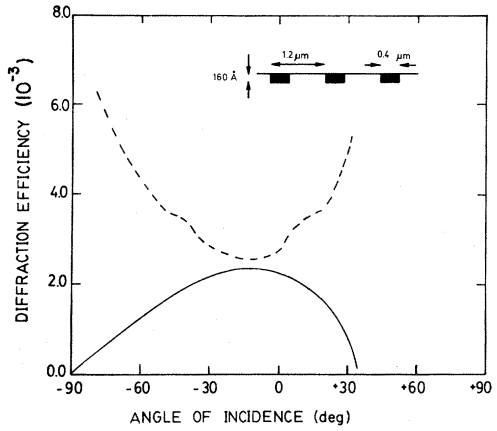

FIG. 8. Diffraction efficiency of a 0.51-μm probe beam from a locally molten germanium surface as depicted in the inset. The dielectric constant of solid germanium at 0.51 μm is $\epsilon_s = 22 + i23$. The plots were calculated as a function of angle of incidence for *s*-polarized (solid curve) and *p*-polarized (dashed curve) beams using the algorithm of Vincent *et al.* (Ref. 32).

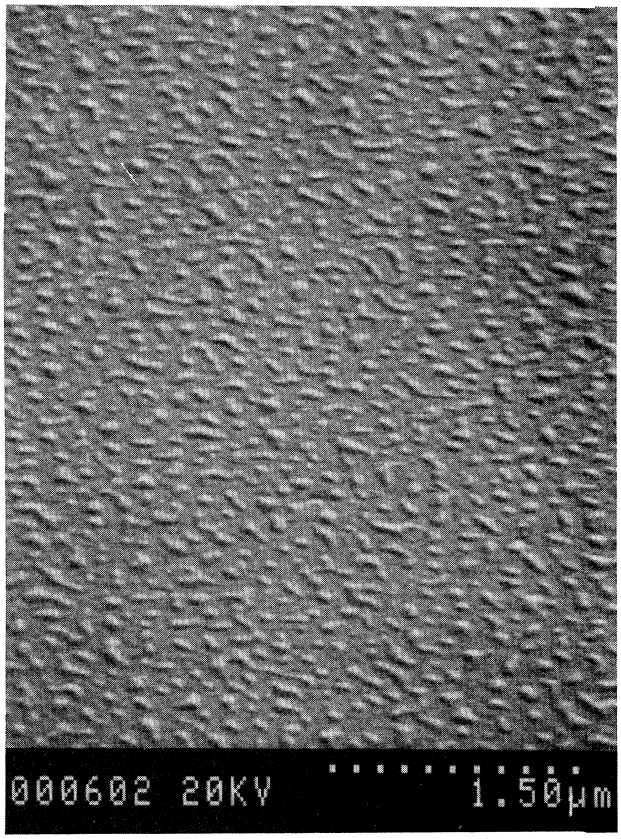

FIG. 9. Electron-microscope picture of the surface of germanium after being irradiated at 30° by two pulses of *s*-polarized, 1.06-μm radiation in fluence regime *A*.

A—*D*) observed with the Ar^+-laser beam normally incident were the same for the two polarizations is consistent with the theory. Of all the surface geometries for which calculations were made, the only one which yields a ratio greater than 2.5 for the *p*- to *s*-polarized components is that shown in Fig. 8, corresponding to a locally molten surface. In addition, the absolute efficiency of the peak transient diffraction spike at normal incidence was routinely as large as 2.5×10^{-3}. This corresponds to the value calculated for the localized molten surface of Fig. 8.

Third, from numerous pairs of oscilloscope traces, as shown in Fig. 2(a), the enhanced reflectivity (which indicates *some* melting has occurred) is observed when and only when a first-order diffraction signal is observed. If a liberal estimate of the error associated with correlating the two signals is allowed, the maximum depth the surface could melt to in a uniform fashion is only 20 Å.

Fourth, and finally, we note that two curious experimental results can be understood in terms of a scenario involving localized melting, and otherwise seem to be virtually inexplicable. The first result is the background, pebblelike structure formed in regime *A* (Figs. 4 and 5); no such structure appears in regimes *B*—*D*. This structure is actually induced by the first one or two laser shots, as evidenced by the photograph taken after just two pulses of *s*-polarized light incident at 30° as shown in Fig. 9. Note that the pebble structure does not change appreciably after the periodic structure is formed; compare Fig. 9 with Figs. 4 and 5. The second result is the somewhat unexpected shot-to-shot development of the diffraction and reflectivity signals observed in regime *A*. With the 1.06-μm beam normally incident on the germanium and the photomultipliers situated to detect the presence of the dominant periodic structure[23] and the specular reflectivity, the specular-reflectivity signal changes very little from shot to shot, while the transient first-order signals increases dramatically for the first 10—15 shots. Although the exact details depend slightly on the irradiation conditions, the same basic behavior is observed whenever the specular reflectivity fails to reach the uniform melt value. During the first one to two pulses there is relatively little transient first-order diffraction observed. From three to six shots, strong diffraction occurs transiently, increasing significantly from shot to shot, but there is little shift in the permanent diffraction level. After six shots, the purely transient component decreases in magnitude and is accompanied by permanent level shifts which are as large as 75% of the peak transient. Once the permanent diffraction has approximately the same magnitude as the largest peak transient observed in the earlier development, only small, gradual transient and permanent level shifts are observed. This corresponds to steady-state fringe patterns which change only slightly from shot to shot.

This behavior can be interpreted as follows. The first few laser pulses induce almost random local melting on the virtually flat initial surfaces left after polishing. This leads to a specularly reflected signal which rises slowly to a value less than 75%, since only a fraction of the surface melts. That inhomogeneous melting would be expected, instead of a homogeneously melted thin layer, can be in-

ferred from a recent stability analysis[33] which shows that thin, molten layers are unstable against fluctuations at almost all wave vectors, and thus can be expected not to develop. Further, Hawkins and Biegelsen[34] have directly demonstrated that when silicon is irradiated with a cw beam of visible or infrared radiation, there is a fluence range between the melting threshold and approximately twice this value for which the surface melts only locally, producing solid lamellae in a molten background. Although these studies are far from complete, they indicate that an assumption of almost random, inhomogeneous melting is not unreasonable; and since, as is shown in the following section, the resolidification of locally molten germanium (or silicon) surfaces has the net effect of raising the central portion of the melted region above the ambient surface level, this assumption allows us to understand both the resulting pebblelike structure, and the low value of the specular reflectivity.

It also is clear that such almost random melting would lead to comparatively little first-order diffraction at any specific wave vector, explaining the lack of strong transient diffraction in the first few shots of the sequence. However, the randomly molten surface resolidifies, leaving a randomly rough surface, one much rougher than the original polished one. Subsequent laser pulses then scatter preferentially into special Fourier components in a manner described by the theory of paper I. This means that many of the areas which melted during the first pulses no longer melt, while other spots, where the periodic inhomogeneous intensity peaks, melt instead. The total fraction of the surface that melts stays approximately the same, but once periodic melting occurs, very strong diffraction of the probe beam from the alternating regions of liquid and solid occurs at positions corresponding to the usual diffraction patterns. The diffraction is predominantly transient for the first few shots, indicating that the periodically molten surface resolidifies almost flat at that stage. Eventually, though, the local resolidification process (discussed in the next section) leads to the growth of permanent structure which rises above the surrounding surface, as shown in the electron-microscope photographs. Since this structure is due to melting only in strips, the early pebble structure remains.

Thus we have confirmed our explanation of the formation of periodic surface structure given in paper II, which was based on the theory presented in paper I, but we have also supplemented it with an important addition: The random surface roughness that was assumed in paper I appears to be, to a large extent, induced by the laser beam itself in the few shots. A more complete understanding of this "laser-induced roughness," and its detailed relation to the inhomogeneities observed in cw experiments, is obviously an important outstanding problem in this field.

We conclude our discussion of regime *A* with the comment that the periodic structures formed at these fluences are distinguished by the fact that they form a steady-state pattern after approximately 20 pulses of the 1.06-μm beam. None of the structures formed at higher fluences attain such an invariant form, confirming our suggestion in paper II that a "steady-state morphology" occurs only when the material melts locally.

B. Regime *D*

We now turn to the higher-fluence regime *D*, where the specular reflectivity remains at the 75% level characteristic of bulk liquid germanium for times longer than 100 ns and for as many as 50 laser pulses. Significant, and sometimes very intense (relative to those observed in regime *A*), first-order transient diffracted signals are observed while the reflectivity is flat-topped at 75%. From the signals as shown in Fig. 2(d), it is clear that the periodic structure responsible for the diffraction exists long after the pump pulse is over. The ratio of *p*- to *s*-polarized diffraction components for the Ar^+-laser beam incident at an angle of 60° is 1.2, characteristic of a modulated air/liquid interface [see Figs. 6(c) and 7]. In this section we demonstrate that these are laser-induced capillary waves, obtain values for the surface tension and kinematic viscosity, and show that the spatial period of the waves is slightly different than those formed in regime *A* at fixed θ.

The most striking aspect of the diffraction, and thus of the structure responsible for it, is its temporally periodic nature. Keilmann[25] reported similar oscillatory diffraction from ripples induced on liquid-mercury surfaces by carbon dioxide laser pulses at a wavelength of 10.6 μm. He showed that the induced ripples were in fact capillary waves by measuring the dispersion related to their natural oscillation period. It is well known[35] that if the wavelength of a perturbation at a liquid surface is much less than $(\alpha/\rho g)^{1/2}$, the dominant restoring force is provided by surface tension. The resulting waves are referred to as capillary waves, and the dispersion of their natural oscillation frequency ω_c is easily shown to be

$$\omega_c=(\alpha/\rho)^{1/2}\kappa_c^{3/2}\,, \tag{1}$$

where α is the surface-tension coefficient of the air/liquid interface, ρ is the density of the liquid, g is the gravitational acceleration, and κ_c is the wave vector of the surface perturbation. Viscous forces cause the amplitude A of the capillary waves to decay as

$$A\sim e^{-\gamma t}\,, \tag{2}$$

where

$$\gamma=(2\eta/\rho)\kappa^2=2\nu\kappa^2\,. \tag{3}$$

Here, η is the shear viscosity and ν is the kinematic viscosity of the liquid.

In our experiments, an upper limit to the period of oscillation that could be accurately measured existed, because, for the fluences used, the germanium could only be kept molten for a maximum of $\sim$200 ns. This also limited the range of decay constants that could be measured; nevertheless, we were able to identify the oscillations as due to capillary waves, as described below.

We used an *s*-polarized, 1.06-μm beam incident at angles between 25° and 60°. The diffracted signals were stored on the oscilloscope screen and photographed on the 50-ns/div scale to measure the decay constant and on the 20-ns/div scale to measure the period of oscillation. The wavelength of the waves was calculated from the spatial frequency of the diffraction monitored by the photomulti-

plier. The period T of one complete oscillation of the diffracted signal [see Fig. 2(d)] corresponds to one-half of the natural oscillation period of the standing wave. The measured natural oscillation frequency, $\omega_c = \pi/T$, as a function of the wave vector to the three-half power [Eq. (1)], is shown in Fig. 10. The slope of the graph is 1.0×10^{-2} $m^{3/2}/s$ with an upside error of $+0.12\times10^{-2}$ $m^{3/2}/s$ and a downside error of -0.07×10^{-2} $m^{3/2}/s$. The fitted line shown in Fig. 10 also passes through the origin. The uncertainty of the measurements is magnified at large frequencies because the absolute reading error remains constant as the period of oscillation decreases.

Three data points were obtained for the decay constant of the oscillations at different wavelengths. Photographs of the transient diffracted signals as shown in Fig. 2(d) were traced and exponential curves were drawn through the peaks on the falling edges. The half-widths of the exponential curves were then plotted as a function of the squared wave vector of the wave [Eq. (3)]. Figure 11 shows the plotted data with a line drawn through the points and the origin.

From Eq. (1), the slope of the graph in Fig. 10 was set equal to $(\alpha/\rho)^{1/2}$. Taking a value of 5.57×10^3 kg/m^3 for the density of molten germanium,[36] the surface tension of molten germanium was estimated at $0.557+0.140$, or -0.075 kg/s^2. Reference 36 gives values of 0.65 and 0.53 kg/s^2 for the surface tension of molten germanium at temperatures of 1000 and 1200 °C, respectively. Since for shallow waves the diffraction intensity is proportional to the square of the amplitude, the slope of the line in Fig. 11 was set equal to $4\nu/\ln 2$ [Eqs. (2) and (3)]. A value of $(1.02\pm0.06)\times10^{-7}$ m^2/s was thus obtained for the kinematic viscosity of liquid germanium. The values of ν given in Ref. 36 are 1.35×10^{-7} and 0.96×10^{-7} m^2/s for temperatures of 950 and 1210 °C, respectively.

The ripples of regime D are therefore clearly identified as capillary waves generated at the air/liquid-germanium interface produced at elevated fluences. If the decay of the capillary-wave activity is not complete by the time the surface resolidifies, a permanent record of the ripples is

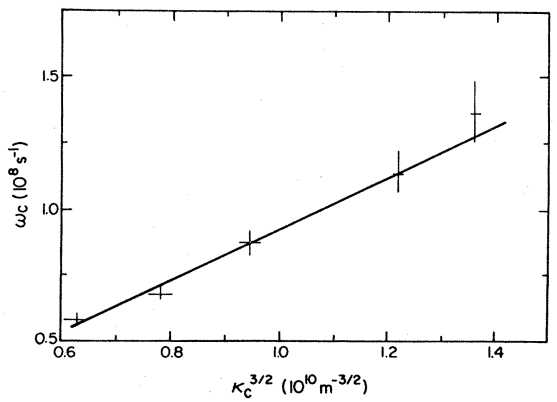

FIG. 10. Measured natural oscillation frequency $\omega_c = \pi/T$ of the capillary waves generated on molten germanium plotted as a function of their wave vector to the three-half power, $\kappa_c^{3/2}$. The straight line represents the best linear fit to the data which also passes through the origin.

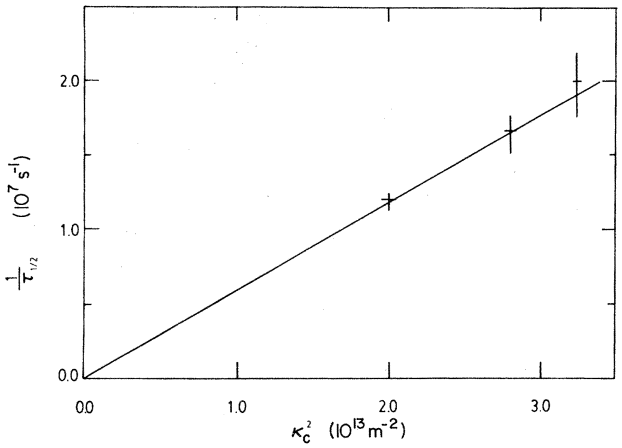

FIG. 11. Measured inverse half-life $1/\tau_{1/2}$ of the squared amplitude of the decaying capillary waves generated on molten germanium as a function of the squared magnitude of the wave vector, κ_c^2. The straight line represents the best linear fit to the data which also passes through the origin.

"frozen" into the surface. Figure 12 shows an electron-microscopic picture of the fringes formed by s-polarized light incident at 45° with a fluence in regime D. Unlike the fringes formed in regime A, these are smoothly varying and sinusoidally shaped, precisely as would be expected from "frozen capillary waves."

It is important to note that, at the elevated fluences required to produce the capillary waves, periodic structures of the types of regimes A—C always form in an annular region, surrounding the hottest part of the sample, where the local fluence is less. Regime D corresponds to the "innermost annular region" discussed in paper II, and, in fact, scattering from laser-induced roughness and periodic structure in the outer regions of the laser spot may be essential in "seeding" capillary waves in the center of the spot, since no transient diffracted signals can be observed from the center for the first 10—12 shots. However, since significant scattering of the argon-ion probe beam in the immediate vicinity of the surface is observed to coincide with the onset of capillary-wave activity, it appears that the feedback mechanism is due to inhomogeneous etching which results from periodic energy deposition beneath the microscopically rough liquid interface (see the following section).

Nonetheless, the presence of both types of fringes within a single spot allows for a sensitive comparison of the spacing of regime-D fringes and the more usual fringes formed by localized melting: By shining the Ar^+-laser beam on the entire region over which fringes are produced, the permanent diffraction patterns from the structures formed in all fluence regimes are superimposed in the far field. When the 1.06-μm beam is s-polarized and incident between 25° and 70°, the composite diffraction pattern consists of two distinct sets of a similar pattern which differ by a well-defined scaling factor.[37] A portion of this pattern near the intersection of the arcs shown in Fig. 1 is shown schematically in the inset of Fig.

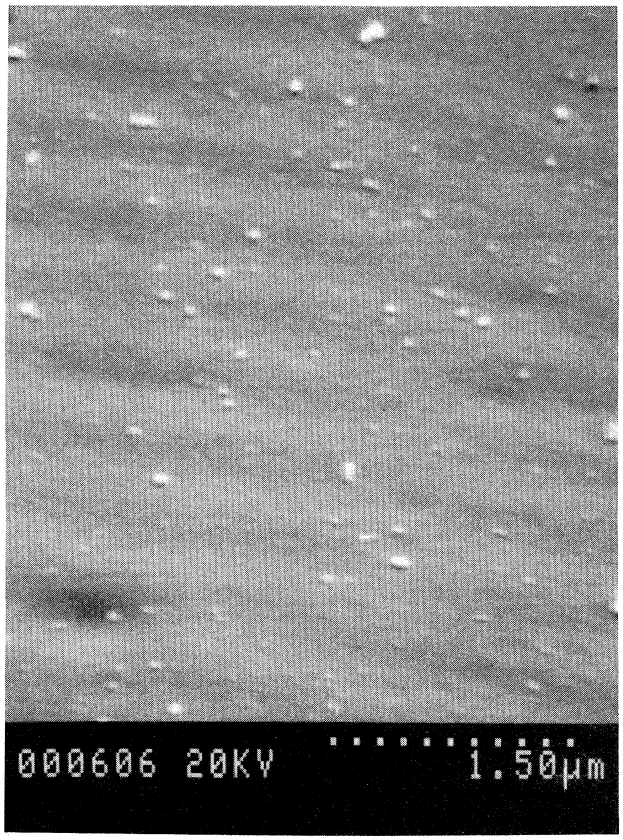

FIG. 12. Electron-microscope picture of the smoothly varying ripples formed by three s-polarized, 1.06-μm pulses incident at 45° with fluences in regime D.

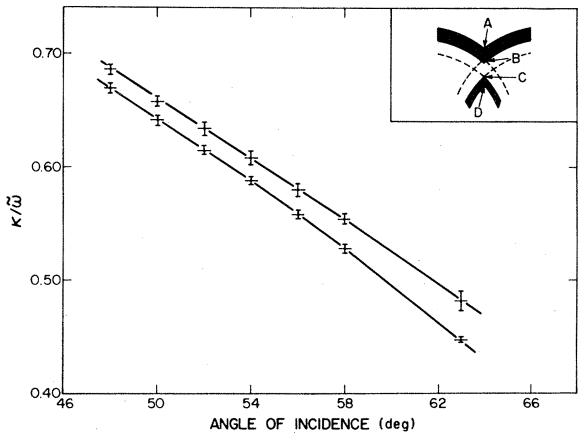

FIG. 13. Plot of the normalized wave vector ($\tilde{\omega} \equiv 2\pi/\lambda$) of induced structure as a function of the $\lambda = 1.06$ μm beam's angle of incidence. The vertical extremities of the data points along the top (bottom) curve correspond to the measured positions of points A and B (C and D) shown in the inset. The inset is a magnified view of the intersection of the two diffraction circles (see paper II). The solid lines represent points at which the variational theory (see paper I) predicts maximum inhomogeneous energy deposition in the case of a liquid (top) and a solid (bottom) germanium surface.

13. The oscillatory transient diffraction shown in Fig. 2(d) was only observed at points along the upper part of the segment shown in Fig. 13, while no oscillatory behavior was observed in the transient diffraction on the lower section. The absolute spatial frequency of the two intersection points were plotted as a function of the incident angle of the 1.06-μm beam, as shown in the main part of Fig. 13. Note that the vertical extremities represent the actual breadth of the lines; the corresponding uncertainty in the measurements was approximately 15% of the total vertical range. The horizontal error bars do represent uncertainties in the incident angle. The implication of these measurements is discussed in the following section, but it is clear that the fringes formed in regime D have a spacing which is consistently and measurably different from the spacing of fringes formed by localized melting.

C. Intermediate regimes

We have seen that the fringes of regimes A and D can, respectively, be identified with localized melting and with capillary waves on a thick, uniformly molten layer. The fringes formed in regimes B and C are intermediate between these two well-defined limits, and are thus both more complicated and probably of less fundamental interest. However, regime B is important in that it confirms the scenario of regime A as localized melting by illustrating precisely what would be expected if the fluence were raised slightly higher so that a uniform, optically thick melt could just be achieved. Regime C is of some interest in that it illustrates how interactions between different regions of the laser spot can, at intermediate fluences, become crucially important, as was noted earlier in paper II.

We first consider regime B, which is characterized by a specular reflectivity which attains the flat-topped, uniform melt value of 75% for a time less than 75 ns [Fig. 2(b)]. A reproducible shot-to-shot evolution is observed for the first 10—15 shots with an increase in the transient diffraction signal, but eventually the specular reflectivity falls below the 75% level and no steady-state patterns are formed. This regime can only be identified in terms of this transient behavior, and was not explicitly recognized in the results presented in paper II.

The most striking feature of the first-order diffraction in regime B are the two large transient spikes which occur only during the rising and falling edges of the specularly reflected signal. As indicated in Fig. 6(b), the level of p-polarized diffraction during the first spike is typically 3.5 to 4 times larger than the s-polarized component, while for the second spike the ratio is between 2.5 and 3.5. During the first few shots there is very little diffraction at all during the flat-topped reflectivity phase. When diffraction is finally observed while the reflectivity is at 75%, the p-polarized component is only 1.2 times as large as the s-polarized component. These results are interpreted as follows, recalling the diffraction calculations presented in Figs. 7 and 8. At fluences just above the level required to uniformly melt the surface, the transition starts from the solid phase and goes through an inhomogeneous molten

phase similar to regime *A* before finally melting uniformly. A modulated liquid/solid interface is then driven to depths greater than the optical skin depth of the probe beam, so that little evidence of the periodicity is recorded in the first-order diffraction. Following the laser pulse, the modulated interface recedes to the surface and resolidifies first in the regions which were less deeply melted. The ratio of *p*- to *s*-polarized diffraction efficiency for the spike corresponding to the resolidification process is less than that observed in regime *A*, likely because the shape of the modulated liquid/solid interface is smoothed through diffusion processes. When it resolidifies, the surface is therefore probably better described by a modulated liquid layer above a solid surface, as opposed to the shape shown in Fig. 8. The calculated *p*- and *s*-polarized diffraction efficiencies indicate that the smoother profile leads to a lower ratio at a 60° angle of incidence.

At slightly higher fluences, in regime *C*, the intensity appears sufficiently high so that a stable, uniform, optically thick molten layer can form immediately: The reflectivity reaches the 75% level and remains there for more than 75 ns during the first one to six shots, while no transient or permanent diffraction is observed. However, the fluence is apparently not high enough to lead to the etching which forms fringes in regime *D*. Instead, as periodic structure gradually develops in the region surrounding the center of the spot, where the local fluence is less, the specular reflectivity takes the form shown in Fig. 2(c), while small transient and permanent diffracted signals are observed. These observations confirm the suggested behavior of the surface in the "intermediate annular region" of paper II: The periodic structure in the surrounding region eventually modulates the intensity enough to induce inhomogeneous melting, which prevents the specularly reflected signal from reaching 75%. The shape of the fringes finally formed (Fig. 14) attest to this, in that although there is evidence of localization associated with inhomogeneous melting, the entire surface has been clearly altered. The transient behavior in regime *C* is, in general, not as reproducible or well defined as that in the other three regimes. No large transient signals are observed, and the ratio of *p*- to *s*-polarized diffraction efficiencies fluctuates randomly from 1 to 2.

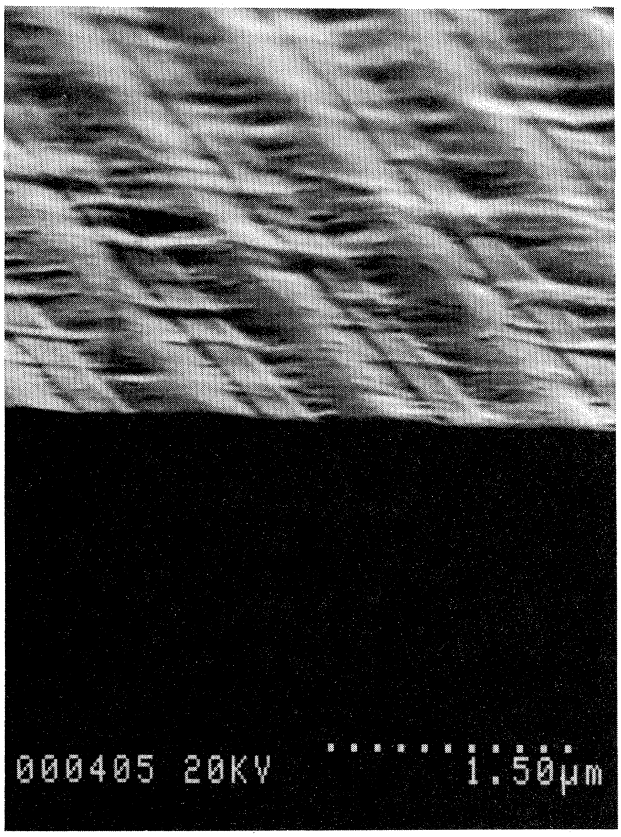

FIG. 14. Electron-microscope picture of the fringes formed by *s*-polarized, 1.06-μm pulses incident at 30° on a germanium surface, with fluences in regime *C*.

IV. FEEDBACK MECHANISMS

The results of experiments described above indicate that there are really two dominant feedback mechanisms involved in the formation of periodic surface structure, a point that has not always been realized in the past.[18,20] The first, an "interpulse feedback mechanism," involves the evolution of the induced surface structure from shot to shot as a given portion of the sample is repeatedly struck by laser pulses; this is particularly significant for fringes formed in regime *A* where the development of a steady-state pattern must be understood. The second, an "intrapulse feedback mechanism," involves the growth of the periodic structure while it is coupled with the incident radiation. This can be expected to be qualitatively different for, say, regime *A* (localized melting) and regime *D* (capillary-wave generation). We discuss these mechanisms in turn in this section.

The main idea embodied in the explanation of the shot-to-shot feedback mechanism is really quite simple. From the scattering theory developed in paper I, the magnitude of a given Fourier component of the intensity generated beneath a rough solid surface is proportional to the amplitude of the same Fourier component of roughness, [see Eqs. (5) and (15) of paper I]. Even though the initial random surface may have no periodic structure, the peaks in the efficacy factor, $\eta(\vec{\kappa},\vec{\kappa}_i)$, indicate that the incident radiation preferentially deposits energy in distinct Fourier components. At sufficiently high fluences this induces either localized melting of the solid surface or waves on the liquid surface (hence the transient diffraction), and a small amount of permanent periodic structure remains after resolidification. At that stage, the spectrum of the surface roughness, $b(\vec{\kappa})$, contains peaks in the same places as $\eta(\vec{\kappa},\vec{\kappa}_i)$. The intensity distribution $I(\vec{\kappa}) = \eta(\vec{\kappa},\vec{\kappa}_i)b(\vec{\kappa})$ generated by the next pulse is thus even stronger in the vicinity of the peaks. This causes greater inhomogeneous energy deposition and further growth of the permanent periodic structure.

The most interesting and important aspect of the shot-to-shot feedback mechanism thus concerns the way in which the melted surface fails to resolidify to a flat profile. Two different explanations have been suggested by

others;[18,20] both involve the growth of a sinusoidal modulation at an interface between air and a uniform layer of molten semiconductor while the laser pulse is incident on the sample. This rippled interface is then "frozen in" as the surface resolidifies. A distinction between the processes which occur in different fluence regimes is not made in either model. The experimental evidence which we obtained indicates that the permanent structure induced following the generation of capillary waves in regime *D* does, in fact, result from the freezing of the waves at the air/liquid interface. However, the idea of frozen waves cannot account for the permanent structures produced at lower fluences for two main reasons. First, the transient diffraction experiments indicate that the periodic structure is formed while the surface at no time melts uniformly. Second, electron-microscopic pictures show that the structures formed are extremely localized; the ridges induced as the result of localized melting occupy less than 30% of the total surface area. They are in no way sinusoidal.

It is, in fact, the localized melting of the stripe less than a micrometer wide, at low fluences, that leads to the characteristic "sombrero-shaped" cross section in Fig. 3. Willis and Emmony[6] reported observing similarly shaped ridges and claimed that this was sufficient evidence to prove that the surface melted only locally. They further suggested that a concave meniscus should form upon localized melting of germanium since the density of the liquid phase, $\rho_l \simeq 5.6\times 10^3$, is higher than that of the solid phase, $\rho_s \simeq 5.3\times 10^3$ kg/m^3.[36] They argued that the "sombrero-shaped" profile occurs because the molten region first resolidifies at the perimeter, "locking a depression into the surface contour." To conserve mass, the central region is eventually raised above the ambient surface level. This simple explanation is qualitatively correct; however, a more detailed description of the processes involved can be given with reference to the work of Surek and Chalmers.[38] Quite unexpectedly, these authors observed that similar "sombrero-shaped" surfaces formed when 1-cm-diam, circular regions of 1-mm-thick germanium and silicon wafers were melted completely through and allowed to resolidify. The one-dimensional nature of their setup provided for a fairly easy interpretation of the results: Following Bradsley, Frank, Green, and Hurle,[39] in thermodynamic equilibrium the net force due to the surface tensions acting normal to the three-phase junction must be zero. Thus, if the resolidification process can be considered to occur in some sense "close" to thermodynamic equilibrium, one would expect there to be a fixed angle between the direction of crystal growth and the vapor/liquid interface, which, in fact, Surek and Chalmers found for a wide range of growth conditions, and which leads to the "sombrero-shaped" surfaces by mass conservation and simple geometry.

Although this explanation is strictly applicable only in the comparatively slow and unidirectional recrystallization process studied by Surek and Chalmers, the striking similarity of the shape we observed to that of those authors indicates that the same basis mechanism is responsible for the growth of structure from the locally melted regions associated with LIPSS. Note that this explanation for the structural growth implies that it occurs *after* the incident laser pulse is over. At higher fluences the waves at the air/liquid interface are generated during the pulse and subsequently frozen.

Turning now to the intrapulse feedback, we note that an exact model of the process by which the periodic surface structure evolves would involve a self-consistent solution of a system consisting of a microscopically rough interface irradiated by polarized radiation which can, in general, induce structural and optical changes in the subsurface region. The complexity of the optically induced material alterations makes this problem quite formidable; however, it is possible to investigate the effects of these material changes on the development of LIPSS in a much simpler, approximate manner. This approach consists of taking the electrodynamic scattering theory and logically incorporating the anticipated material alterations using an "iterative feedback" technique. If the inhomogeneous intensity at a given Fourier vector $I(\vec{\kappa})$ induces spatially periodic changes in the material and/or optical properties of amplitude $U(\vec{\kappa})$, which, in turn, alter the scattered intensity, the dynamics of the coupled system can be described by the equations

$$\frac{\partial U(\vec{\kappa})}{\partial t}=\alpha_1 I(\vec{\kappa}),\quad I(\vec{\kappa})=\alpha_2 U(\kappa)\,, \tag{4}$$

where α_1 and α_2 represent the (linearized) coupling coefficients which describe the effect of the radiation on the material, α_1, and the effect of the periodic material perturbation on the scattering efficiency, α_2. The solution of this set of equations implies that exponential growth of both U and I can be expected if α_1 and α_2 are positive.

The basic concepts involved in the intrapulse feedback process are most simply demonstrated in the case of regime *D*. Figure 15 shows a plot of the spatial Fourier spectrum of field intensity just beneath a randomly rough liquid-germanium surface irradiated by *s*-polarized 1.06-μm radiation incident at 52°. The orientation of the normalized wave vector is parallel to the incident field's po-

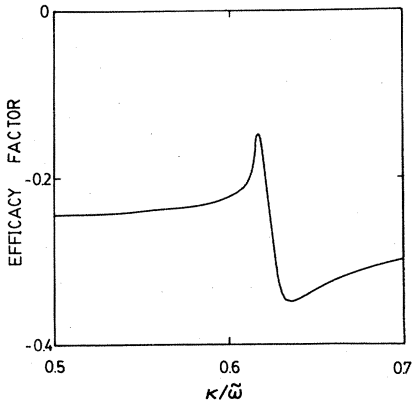

FIG. 15. Efficacy factor $\eta(\vec{\kappa};\vec{\kappa}_i)$ (see paper I) as a function of $\kappa/\tilde{\omega}(\omega=2\pi/\lambda)$ for *s*-polarized, $\lambda=1.06$ μm radiation incident at 52° on a molten-germanium surface. The direction of $\vec{\kappa}$ is parallel to the incident electric field. The dielectric constant of molten germanium at $\lambda=1.06$ μm is $\epsilon_l=-32+i72$.

larization and the calculation was done using the formulas presented in paper I. Note that the shape of the peaked structure is characteristically different from that seen in similar calculations performed for randomly rough solid surfaces, as shown in paper II. This is due to the fact that, in the liquid case, the dominant scattered-field structure is due to a surface plasmon, while in the solid case it is due to a radiation remnant.[22] The broad dip corresponds to the position of maximum inhomogeneous energy deposition in Fourier space and the negative phase indicates that the field intensity is greatest in the "valleys" of the roughness. As was mentioned in Sec. III, the fluence threshold for observing capillary waves in regime D coincides with the visual observation of anomalously strong scattering of the argon-ion probe beam just in front of the sample surface. This, coupled with the fact that the intensity is greatest in the "valleys" of the roughness, suggests that the component of random roughness on the liquid surface at the wave vector corresponding to the dip in Fig. 15 should grow in amplitude faster than any other roughness component due to a preferential etching mechanism. Thus the interaction of the radiation with the rough liquid surface at fluences corresponding to regime D can be characterized, within a linearized approximation, by a positive α_1 in Eqs. (4). As long as the height of the ripple remains much less than the wavelength of light, the inhomogeneous intensity scales with the amplitude of the ripple,[22] so that the coefficient α_2 in Eqs. (4) is also positive, and an exponential growth of small-amplitude roughness can be expected, with the maximum growth rate occurring at the wave vector corresponding to the position of the broad peak in Fig. 15. An obvious extension of this work would be to quantitatively measure the growth rate of the capillary waves and to theoretically estimate a value for the coefficient α_1 in order to obtain a growth rate with which to compare with experiment.

Before discussing the intrapulse feedback process involved in regime A, it is appropriate here to point out that the solid line drawn through the top set of data points in Fig. 13 was obtained by plotting the position of the maximum inhomogeneous energy deposition from graphs similar to Fig. 15 drawn for various angles of incidence. The solid line through the bottom set of data in Fig. 13 was obtained in the same way from plots of the inhomogeneous energy-deposition spectrum beneath randomly rough surfaces of solid germanium. The good agreement between theory and experiment indicates that the structures formed in fluence regimes A–C are due to radiation-remnant field structures, while the capillary waves are the results of interference of the incident beam with surface plasmons at the air/liquid interface.

The intrapulse feedback mechanism corresponding to regime A is much more complicated than the preferential etch mechanism of regime D. In the capillary-wave case, the SEM work indicates that the ripples are smooth, nearly sinusoidally shaped, and although an inhomogeneous phase transition is involved, the vapor phase can be assumed, to a good approximation, not to influence the electrodynamics. It seems probable that Eqs. (4) actually provide an accurate description of at least the initial phase of the capillary-wave growth dynamics. In contrast, as shown in the preceding section, regime A is characterized by a localized, periodic phase transition in which *both* phases *must* be treated in considering the electrodynamics. We feel that Eqs. (4) can really only be used on a conceptual basis when discussing regime A's growth dynamics since neither the geometry nor the nature of the material changes lend themselves to a linearized, harmonic analysis. We have nevertheless found it useful to pursue an understanding of the growth processes involved in regime A within the context of the iterative feedback concept implicit in Eqs. (4). The results of our investigation into this matter warrant discussion here since they clearly identify the important role which local-field effects play in the overall process.

Consider the problem of explaining how the periodic molten regions, which lead to the transient spike in the first-order diffraction, as illustrated in Fig. 2(a), develop under the influence of a pump pulse normally incident on a germanium surface which has already been struck by three or four similar pulses and hence already has a small-amplitude surface modulation similar to that shown in Fig. 4. Qualitatively, what must happen is that the incident energy is preferentially deposited in the regions which are slightly raised as the result of previous localized melting. Eventually, these regions remelt and the increased diffraction efficiency resulting from the abrupt, periodic discontinuity in the dielectric constant leads to greater preferential energy deposition in the molten regions, which causes them to expand, leading to a further increase in the scattering efficiency. The degree to which the scattering efficiency increases must be greatest for periodic roughness with wave vectors corresponding to those which actually develop spontaneously for a given angle of incidence.

In trying to model this process, if one attempts to simplify the situation by adopting a sinusoidal shape for the initial roughness, the "hills" correspond to the portion of the surface which has been raised as the result of previous localized melting (see Fig. 3). However, the pump-field intensity developed just beneath such a surface is a maximum underneath the "valley" of the ripple. This leads to an immediate contradiction since it implies that the surface would melt in the regions between those where it had melted under the influence of previous pulses. The sinusoidal model is therefore too crude an approximation for the localized ridges of Fig. 3, and, as an alternative, we take a periodic array of solid-germanium rectangular strips placed on top of a planar germanium surface with dimensions as illustrated in the inset of Fig. 16. The real-space field-intensity distribution produced just beneath the flat surface was obtained through a numerical solution of Maxwell's equations for normally incident 1.06-μm radiation and the result is shown in Fig. 16. The obviously strong local fields result in a maximum intensity in the immediate vicinity of the raised region, and hence one can understand how the surface melts first in the regions which have previously melted and subsequently risen above the ambient surface level.

Attempts to use sinusoidal surfaces to demonstrate that the scattering efficiency increases most upon local melting of rough surfaces at wave vectors corresponding to those

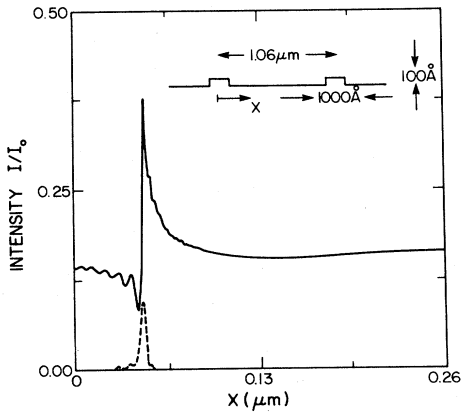

FIG. 16. Plot of the normalized real-space intensity just beneath the solid selvedge shown in the inset. The 1.06-μm radiation is normally incident and polarized parallel to the wave vector of the roughness. The solid and dashed curves represent the contributions to the total intensity made by the $\hat{x}$ and $\hat{z}$ components of the electric field, respectively, where $\hat{z}$ points in the vertical direction in the inset.

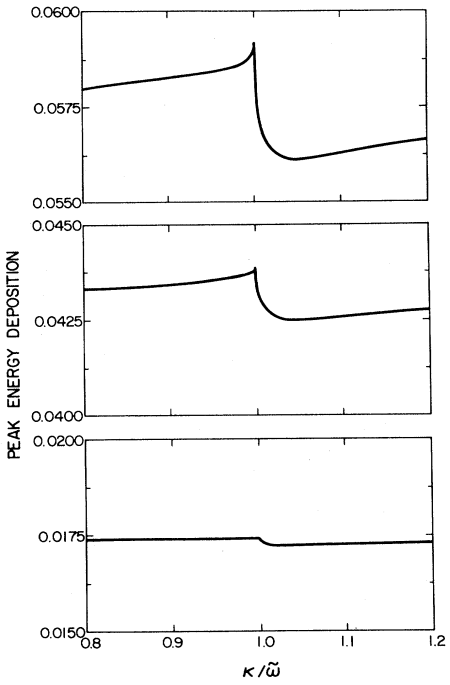

FIG. 17. Peak local intensity as a function of $\kappa/\tilde{\omega}$, where κ is the wave number of the periodic roughness and $\tilde{\omega}=2\pi/\lambda$, for the cases mentioned in the text: (i) is the bottom curve, (ii) is the middle curve, and (iii) is the top curve.

at which structure is known to be produced, were successful under certain assumed irradiation conditions, but unsuccessful for others. By again incorporating local-field effects, a much more satisfying demonstration of the effect was obtained. This approach consists of comparing the value of the peak local intensity (from plots as shown in Fig. 16) as a function of the wave vector of the periodic surface for three different types of ridges: (i) solid germanium of dimensions shown in Fig. 16, (ii) molten germanium of the same dimensions, and (iii) liquid germanium of slightly larger ridge dimensions. The peak field intensity was calculated using a direct extension of the variational theory described in paper I, applied to the case of a periodic, deterministic selvedge region.[40] Figure 17 shows a plot of the peak local-field intensity just beneath the flat solid surface for the above three cases, calculated for a 1.06-μm beam normally incident with its polarization parallel to the wave vector of the surface roughness. Note that at each stage the absolute intensity increases, and that the increase is greatest at the normalized wave vector ($\kappa/\tilde{\omega}\sim 1$) at which damage is, in fact, induced under these illumination conditions.[23] Similar results are obtained for other irradiation conditions, including those for which a sinusoidal model completely fails to show the effect.

In closing this section, we reiterate that the phenomenological incorporation of optically induced material changes via the iterative feedback technique is only a first step towards a more rigorous, self-consistent solution of the coupled radiation-material system. Nevertheless, this simple approach has demonstrated that localized melting of a solid semiconductor and preferential etching of a liquid-semiconductor surface both provide feedback mechanisms by which certain Fourier components of the scattered fields may grow in amplitude while the laser is incident on the sample. It has also shown that local-field effects in the vicinity of the perturbed regions should not be overlooked in a more detailed solution of the problem.

V. CONCLUSIONS

In this paper we have experimentally and theoretically illustrated the dynamical processes associated with the interaction of a coherent, polarized laser beam with a material surface. Emphasis has been placed on the growth kinetics of periodic surface structures, using Ge as a prototypical material. Certain aspects may not be the same for other materials which have different properties, such as their temperature and phase-dependent dielectric constants. In papers I and II we successfully demonstrated and modeled the rich spatial spectra observed on solid surfaces. Here, we have shown the detailed surface morphology that results from inhomogeneous energy deposition and how this morphology changes with the laser fluence level. We have identified four qualitatively different regimes of LIPSS as a function of fluence level. These range from the low-fluence regime of spatially periodic melting induced by inhomogeneous energy deposition on a totally solid material, to a high-fluence regime of periodic etching and induced capillary waves on a totally liquid surface. Through these regimes the cross-sectional shape of the induced ripples changes equally dramatically, from localized, "sombrero-shaped" regions at low fluence, to sinusoidal-type profiles at high fluence. The spatial period of the ripples also depends on the fluence; those formed as the result of capillary-wave generation have spacings determined by the surface plasmon excited at the liquid/air interface, while the spacing of those produced at lower fluences is dictated by radiation remnants generated at the solid/air interface. In these various regimes

we have also identified the role of intra- and interpulse feedback. In doing so we have semiquantitatively investigated the full electromagnetic-material interaction, taking into account inhomogeneities of the surface phase and local-field effects for microscopic structures. With respect to future progress in the understanding of the dynamics, we feel that only in regime *D*, which involves a preferential etching mechanism that leads to capillary waves on an otherwise uniform liquid, is there a potential of obtaining a more quantitative understanding of the feedback process. The other regimes of LIPSS's are more difficult to model, because, for example, of the integral role which periodic melting plays in the feedback process. In particular, it is not likely that a simple exponential growth model for the periodic structure formed at low fluences can be obtained.

Our conclusions concerning the origin and dynamics of LIPSS differ substantially from two other recently proposed models—by Ehrlich, Brueck, and Tsao,[18] and Zhou, Fauchet, and Seigman.[20] Each of these groups presents a single model to explain the development of LIPSS on semiconductor surfaces; no distinction is made between the structures produced in different fluence regimes. In these other models, the surface is assumed to melt uniformly to a small ($\lesssim$500 Å in Ehrlich *et al.*) or large (semi-infinite in the Zhou *et al.*) depth before any periodic structure develops. Our results definitely show that this uniform-melting hypothesis is not applicable to the fringes formed at low fluences (regime *A*). At higher fluences (in regime *D*), where the surface definitely does melt uniformly, we have demonstrated that the periodic structure results from the frequency of capillary waves generated at the vapor/liquid interface. The uniform-melt—layer model of Ehrlich, Brueck, and Tsao[18] does not consider capillary waves at all. Zhou, Fauchet, and Seigman[20] do consider the development of a ripple at the vapor/liquid interface, but they imply that an inhomogeneous thermal-expansion mechanism most likely allows the ripples to grow under the radiation field. This mechanism requires more energy to be deposited in the "hills" rather than the "valleys" of the ripples, whereas the preferential etch mechanism which we propose implies the energy is primarily deposited in the "valleys." By comparing the actual spacing of the ripples formed in regime *D* (see Fig. 13) with the spacing predicted by both Zhou *et al.*[41] and our own electrodynamic calculations (see Fig. 15), it is clear that the energy is actually preferentially deposited in the "valleys" of the ripples, thus supporting the preferential etching mechanism.

In summary, we have studied the fluence dependence and growth kinetics of LIPSS's on Ge and have presented a general model which accounts for the observations made to date.[42]

ACKNOWLEDGMENTS

We gratefully acknowledge financial support from the Natural Sciences and Engineering Research Council of Canada for this work as well as for J.F.Y.

[1]See *Laser-Solid Interactions and Transient Thermal Processing of Materials,* edited by J. Narayan, W. L. Brown, and R. A. Lemons (North-Holland, New York, 1983).
[2]P. Baeri, S. V. Campisano, G. Foti, and E. Rimini, Phys. Rev. Lett. **41**, 1246 (1978).
[3]R. F. Wood and G. E. Giles, Phys. Rev. B **23**, 2923 (1981).
[4]M. Lax, Appl. Phys. Lett. **33**, 786 (1978).
[5]M. Birnbaum, J. Appl. Phys. **36**, 3688 (1965).
[6]L. J. Willis and D. C. Emmony, Opt. Laser Technol. **7**, 222 (1975).
[7]M. Oron and G. Sorensen, Appl. Phys. Lett. **35**, 782 (1979).
[8]R. M. Walser, M. F. Becker, D. Y. Sheng, and J. G. Ambrose, in *Laser and Electron Beam Interactions and Material Processing,* edited by T. J. Gibbons, W. Hess, and T. Sigmon (Elsevier, New York, 1981).
[9]J. F. Young, J. E. Sipe, M. I. Gallant, J. S. Preston, and H. M. van Driel, in *Laser and Electron Beam Interactions with Solids,* edited by B. R. Appleton and G. K. Celler (North-Holland, Amsterdam, 1982), p. 233.
[10]N. R. Isenor, Appl. Phys. Lett. **31**, 148 (1977).
[11]H. J. Leamy, G. A. Rozongi, T. T. Sheng, and G. K. Celler, Appl. Phys. Lett. **32**, 535 (1978).
[12]G. N. Maracus, G. L. Harris, C. A. Lee, and R. A. McFarlane, Appl. Phys. Lett. **33**, 453 (1978).
[13]P. A. Temple and M. J. Soileau, IEEE J. Quantum Electron. **QE-17**, 2067 (1981).
[14]A. K. Jain, V. N. Kulkarni, D. K. Sood, and J. S. Uppal, J. Appl. Phys. **52**, 4882 (1981).
[15]S. R. J. Brueck and D. J. Ehrlich, Phys. Rev. Lett. **48**, 1678 (1982).
[16]Daniel J. Ehrlich, Richard M. Osgood, Jr., and T. F. Deutsch, IEEE J. Quantum Electron **QE-16**, 1233 (1980).
[17]L. D. Hess, G. Eckhardt, S. A. Kokorowski, G. L. Olson, A. Gupta, Y. M. Chi, J. B. Valdez, C. R. Ito, E. M. Nakaji, and L. F. Lou, in *Laser-Solid Interactions and Transient Thermal Processing of Materials,* Ref. 1, p. 337.
[18]D. J. Ehrlich, S. R. J. Brueck, and J. Y. Tsao, Appl. Phys. Lett. **41**, 630 (1982).
[19]P. M. Fauchet and A. E. Siegman, Appl. Phys. Lett. **40**, 824 (1982).
[20]Zhou Guosheng, P. M. Fauchet, and A. E. Siegman, Phys. Rev. B **26**, 5366 (1982).
[21]F. Keilmann and Y. H. Bai, Appl. Phys. A **29**, 9 (1982).
[22]J. E. Sipe, J. F. Young, J. S. Preston, and H. M. van Driel, Phys. Rev. B **27**, 1141 (1983).
[23]J. F. Young, J. S. Preston, H. M. van Driel, and J. E. Sipe, Phys. Rev. B **27**, 1155 (1983).
[24]M. J. Soileau and Eric W. van Stryland, in *Proceedings of the Fourteenth Annual Symposium on Optical Materials for High Power Lasers, Boulder, Colorado, 1982,* U.S. National Bureau of Standards, edited by A. H. Guenther (U.S. GPO, Washington, D.C., 1982).
[25]F. Keilman, Phys. Rev. Lett. **51**, 2097 (1983).
[26]H. M. van Driel, J. E. Sipe, and J. F. Young, Phys. Rev. Lett. **49**, 1955 (1982).
[27]R. J. Archer, J. Electrochem. Soc. **104**, 619 (1957).

[28]J. V. White, J. Opt. Soc. Am. **32**, 285 (1942).
[29]Jeff F. Young, J. S. Preston, J. E. Sipe, and H. M. van Driel, Phys. Rev. B **27**, 1424 (1983).
[30]*American Institute of Physics Handbook,* edited by D. E. Gray (McGraw-Hill, New York, 1972).
[31]J. N. Hodgson, Philos. Mag. **6**, 509 (1961).
[32]P. Vincent, M. Neviere, and D. Maystre, Nucl. Instrum. Methods **152**, 123 (1978).
[33]Jeff F. Young, J. E. Sipe, and H. M. van Driel, in *Laser Controlled Chemical Processing of Surfaces,* edited by A. W. Johnson and D. J. Ehrlich (Elsevier, New York, 1984).
[34]W. G. Hawkins and D. K. Bieglelsen, Appl. Phys. Lett. **42**, 358 (1983).
[35]L. D. Landau and E. M. Lifshitz, *Fluid Mechanics* (Pergamon, London, 1959).
[36]V. M. Glazov, S. N. Chinzhevskaya, and N. N. Glagoleva, *Liquid Semiconductors* (Plenum, New York, 1969).
[37]Jeff F. Young, J. E. Sipe, and H. M. van Driel, Opt. Lett. **8**, 431 (1983).
[38]T. Surek and B. Chalmers, J. Cryst. Growth **29**, 1 (1975).
[39]W. Bardsley, F. C. Frank, G. W. Green, and D. T. J. Hurle, J. Cryst. Growth **23**, 341 (1974).
[40]J. E. Sipe, Jeff E. Young, and H. M. van Driel (unpublished).
[41]We note that the formula with Zhou, Fauchet, and Siegman (Ref. 20) (ZFS) derive [their Eq. (14)] for the first-order amplitude of the electric field scattered from a sinusoidally rippled interface differs slightly from the equation which we (Ref. 22) and others (Reference 18 and F. Toigo, A. Marvin, V. Celli, and N. R. Hill [Phys. Rev. B **15**, 5618 (1977)]) obtain for sinusoidal surfaces. In plots of the inhomogeneous energy depositions as a function of the roughness wave vector (similar to Fig. 17 in this paper), the ZFS's formula yields curves of much the same shape as we obtain, but the absolute values, and in certain cases the phase ($+1$ or -1) of the scattered field at the local extrema of the plots, are different. We feel this discrepancy is worth noting because the phase of the scattered fields near the extrema of the energy deposition in $\vec{\kappa}$ space are crucial to discussions of feedback mechanisms, as we point out in the text.
[42]At this point we would like to correct some errors which appeared in paper I of this series (Ref. 22). In particular, (i) the integral on the right-hand side of Eq. (3.11) should be multiplied by $-\frac{1}{4}$, (ii) the numerator of Eq. (4.15) should include a term $-3z\vec{p}\hat{z}$, and (iii) the first term on the right-hand side of Eq. (4.21) should be multiplied by -1. We apologize for not detecting these errors earlier.

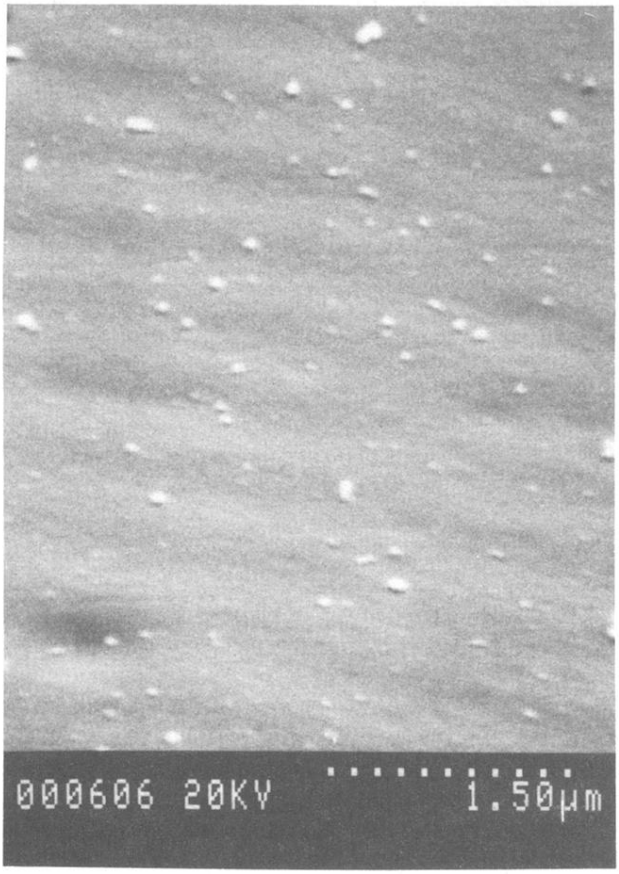

FIG. 12. Electron-microscope picture of the smoothly varying ripples formed by three *s*-polarized, 1.06-μm pulses incident at 45° with fluences in regime *D*.

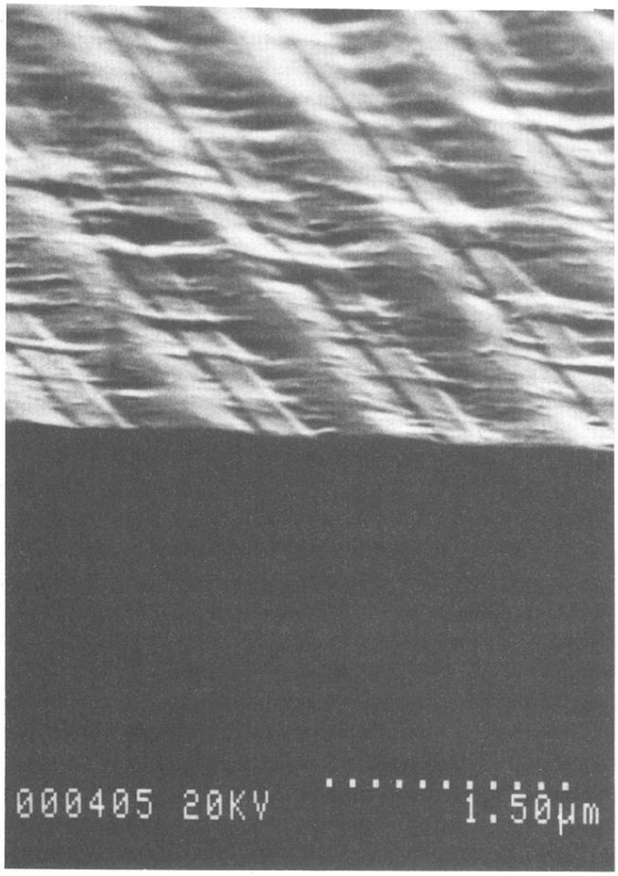

FIG. 14. Electron-microscope picture of the fringes formed by *s*-polarized, 1.06-μm pulses incident at 30° on a germanium surface, with fluences in regime *C*.

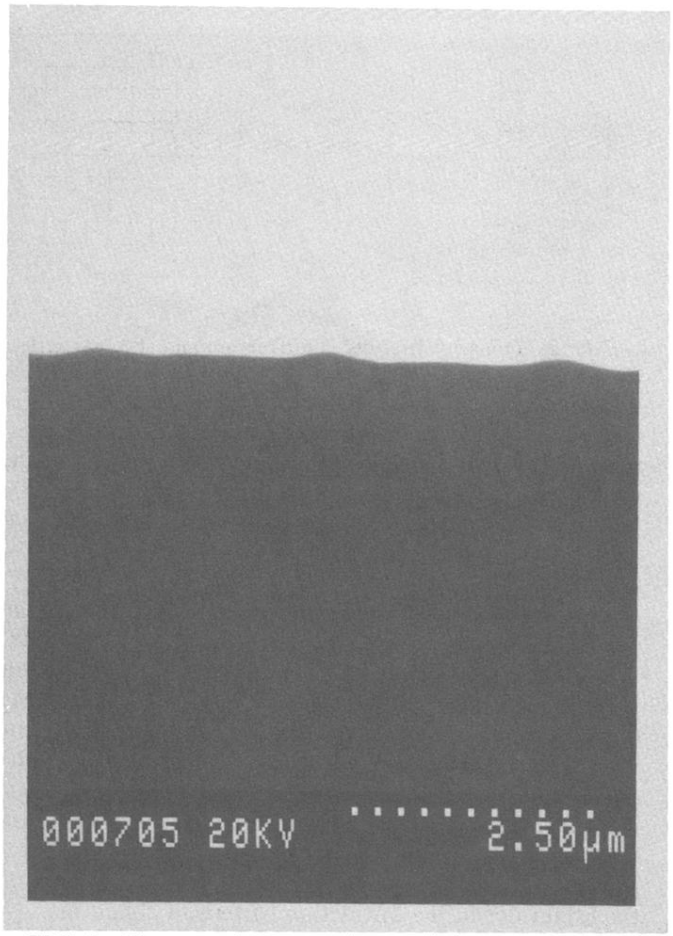

FIG. 3. Electron-microscope picture of the cross section of fringes formed by p-polarized, 1.06-μm pulses incident on germanium at 60° in regime A.

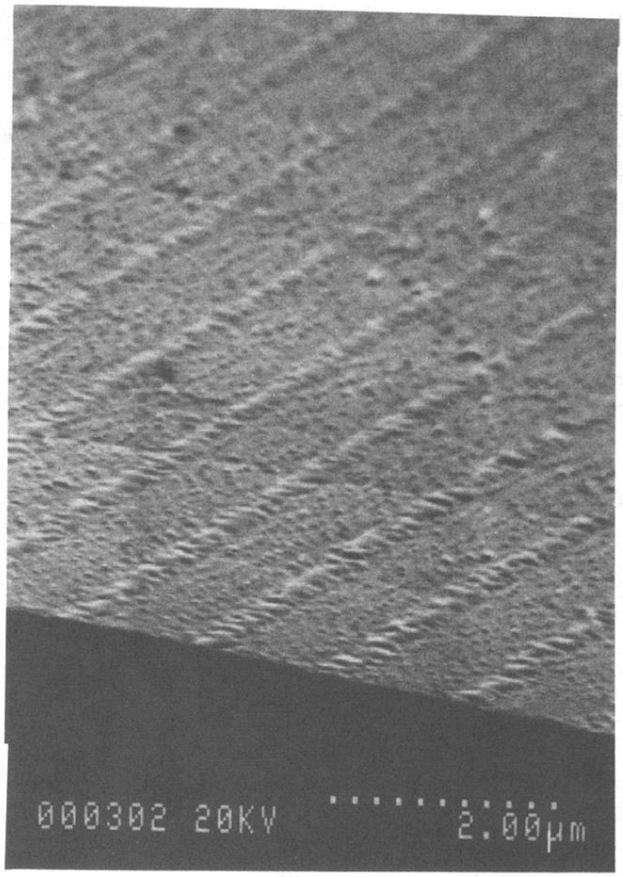

FIG. 4. Electron-microscopic picture of fringes formed by 20 *s*-polarized pulses of 1.06-μm radiation incident at 30° in fluence regime *A*.

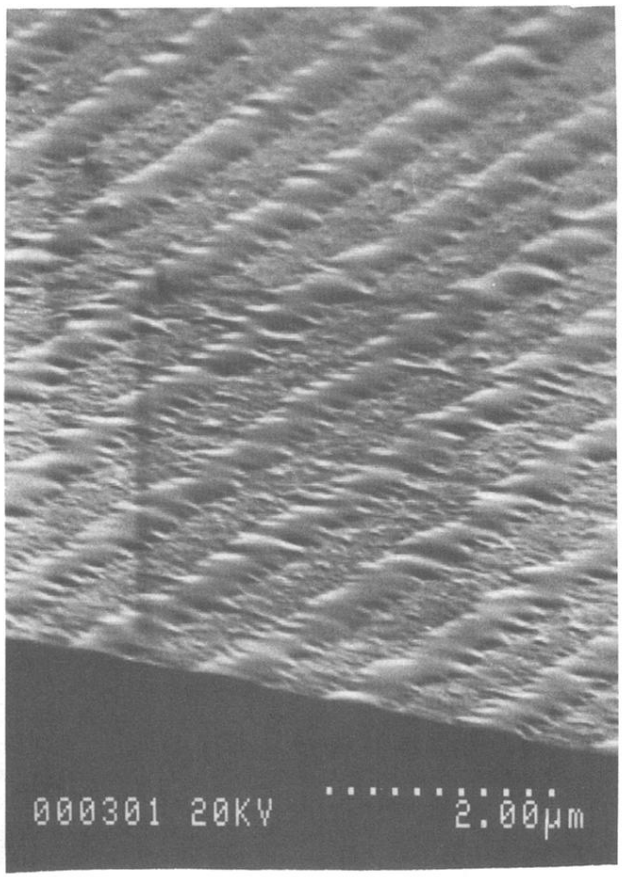

FIG. 5. Electron-microscopic picture of fringes formed under the conditions of Fig. 4, but at higher fluence, although still in regime *A*.

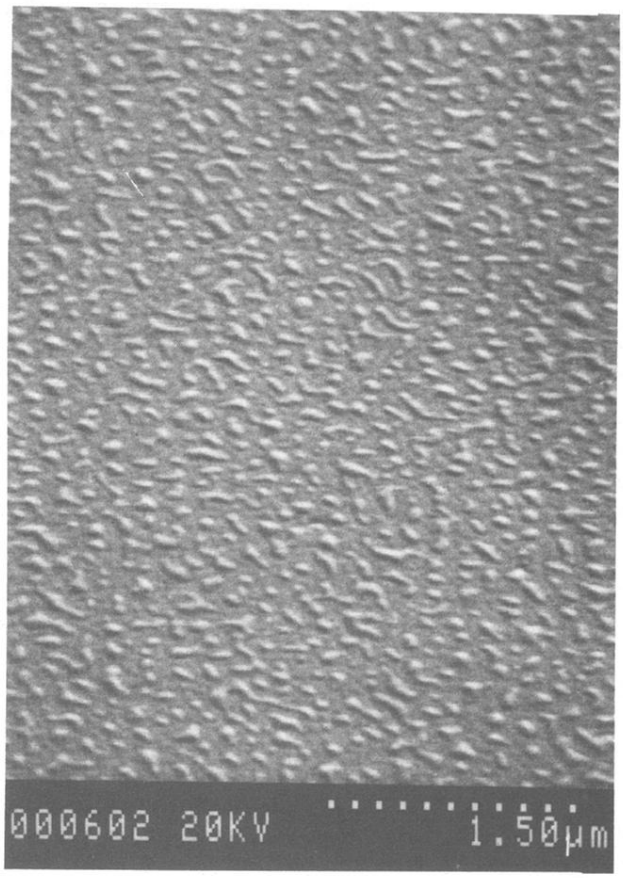

FIG. 9. Electron-microscope picture of the surface of germanium after being irradiated at 30° by two pulses of *s*-polarized, 1.06-μm radiation in fluence regime *A*.